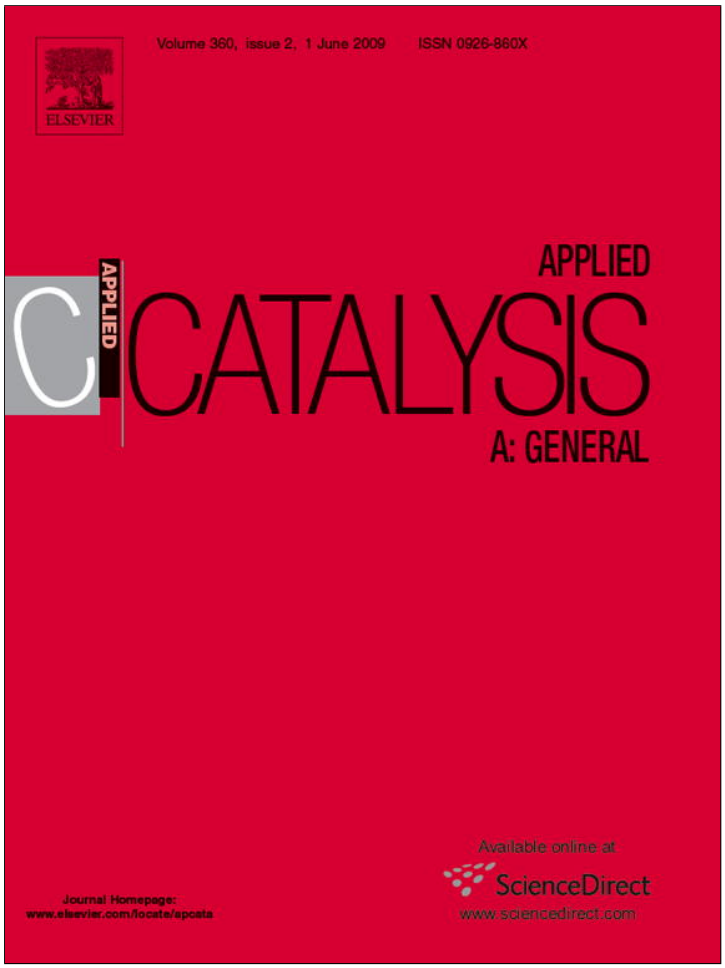

Applied Catalysis A: General 360 (2009) 107–119

Contents lists available at ScienceDirect

Applied Catalysis A: General

journal homepage: www.elsevier.com/locate/apcata

Review

Steam resistant CoLa-mordenite catalysts for the SCR of NO_x with CH_4

Laura Gutierrez *, Eduardo A. Lombardo

Instituto de Investigaciones en Catálisis y Petroquímica – INCAPE - (FIQ,UNL-CONICET), Santiago del Estero 2829, 3000 Santa Fe, Argentina

ARTICLE INFO

Article history:
Received 19 December 2008
Received in revised form 12 March 2009
Accepted 25 March 2009
Available online 2 April 2009

Keywords:
Mordenite stability
Co-mordenite deactivation
Zeolite hydrothermal stability
NO_x elimination

ABSTRACT

The stabilization of Co-mordenite catalysts through lanthanum exchange is reported here. The effect of exchange order and calcination conditions upon the reduction of NO_x to N_2 at 500 °C was tracked during 400 h on a stream containing NO_x, CH_4, O_2 and 10% H_2O. Both the fresh and used catalysts were characterized through TPR, Raman spectroscopy, FTIR spectroscopy using CO as probe molecule, and XPS. These techniques revealed that the CoLa-mordenite catalysts which were not affected by the severe hydrothermal treatment showed no sign of Co or La migration out of the exchange positions. Instead, those that rapidly deactivated showed the formation of cobalt oxides and, in some cases, the migration of the cations to other exchange positions. The presence of exchanged lanthanum seems to preserve the integrity of the zeolite structure preventing the migration of cobalt ions with the subsequent formation of cobalt oxides which favors the reaction of methane with O_2, thus decreasing N_2 production.

Contents

1. Introduction

The selective catalytic reduction of nitric oxides by hydrocarbons has been widely investigated since the initial reports by Held et al. [1] and Iwamoto et al. [2], almost two decades ago. Co-zeolites

* Corresponding author. Tel.: +54 342 4536861; fax: +54 342 4536861.
E-mail address: lbgutier@fiq.unl.edu.ar (L. Gutierrez).

0926-860X/$ – see front matter © 2009 Elsevier B.V. All rights reserved.
doi:10.1016/j.apcata.2009.03.031

(mainly ZSM-5, mordenite and ferrierite) are of particular interest because of their activity and selectivity when using methane [3]. But by now, it is well-known that zeolites are not stable under rigorous conditions (gas streams containing water at high temperature). For this reason the use of zeolite-based catalysts is limited.

Co-zeolite deactivation has been studied by several authors, but none of these studies evaluate the catalysts for more than 50 h on stream [4–8]. Basically, they conclude that exposure to water vapor at high temperatures irreversibly depresses the activity because some structural changes occur in the solids. The most important ones are the following:

- Dealumination, i.e., removal of the tetrahedral Al^{3+} ion from the zeolite lattice.
- Formation of metal oxides, loss of the dispersion and migration of exchanged cations to highly coordinated non-accessible locations.

It is worth noticing that all these changes are in intimate relation with each other.

It has been shown that the addition of a second metal to Co-zeolites, such as Pd or Pt, improves their stability and decreases the deleterious effect of water [9–14]. However, the durability of zeolite-based catalysts is not yet long enough to make its use economically feasible in the treatment of combustion exhaust gases.

Rare-earth (RE) ions play an important role in the stabilization of Y-zeolites used in the fluid catalytic cracking (FCC) of petroleum distillates. These cations are responsible for improving acidity, cracking activity, and thermal stability [15]. The latter has been associated with the formation of lanthanum-hydroxyl species in zeolite channels, following thermally induced hydrolysis of the $[RE(H_2O)_n]^{3+}$ cations upon calcination [16] and their migration to smaller cages [17–21].

On the other hand, Bao and co-workers [22,23] reported a theoretical approach to the improvement in hydrothermal stability of La-modified ZSM-5 zeolite. They employed density functional calculations to investigate the location and binding of lanthanum cations, i.e., $La(OH)_2^+$ on H-ZSM-5. They found that the charges on both Al and O atoms in La-ZSM-5 show an increase compared to H-form zeolite, which would undoubtedly lead to a stronger mutual interaction and, hence, enhance the stability of the $[AlO_4]^-$ anion. Moreover, $La(OH)_2^+$ seems to have thickened the zeolite framework, which can effectively retard the process of dealumination.

In this work, we studied the stabilizing effect of La-exchanged in the mordenite lattice which also contains Co as the active element for the SCR of NO_x with methane. The stability was tested under very severe conditions (500 °C, 10% of water, 400 h on stream).

Fresh and used catalysts were characterized by XRD, XPS, Raman, TPR, FTIR, BET and CO-FTIR adsorption to elucidate the role of lanthanum into the matrix and the changes of the Co-H-mordenite structure and the evolution of cobalt species present in each solid.

2. Experimental

2.1. Catalyst preparation

The catalysts were prepared by ion exchange starting from Na-mordenite (NaM) (Zeolyst CBV 10A, Si/Al = 6.5). The ion exchanged forms, H-mordenite (HM) and Co-H-mordenite (CoHM) were prepared following the procedure reported by Gutierrez et al. [24]. An aliquot of HM was exchanged with a solution of $Co(CH_3COO)_2$ to obtain CoHM. Then, an aliquot of CoHM was contacted with a $La(NO)_3$ solution during 36 h at 25 °C. The solids denominated CoLaHM-400, CoLaHM-500 and CoLaHM-600 were calcined at 400, 500 and 600 °C prior to La exchange.

Table 1
Compositions of the synthesized catalysts.

Catalyst	Co (wt%)[a]	La (wt%)[a]	%IE[b]	Co/La[c]
LaHM	–	1.85	12	–
CoHM[d]	1.15	–	18	–
CoLaHM[d]	0.96	0.96	19	2.02
CoLaHM-400	1.15	1.04	25	2.61
CoLaHM-500	1.69	1.22	35	3.45
CoLaHM-600	1.93	1.24	40	3.74
LaCoHM	2.70	2.20	60	3.01
La/HM	–	1.00		–
Co/HM	2.91	–		–
La_2O_3/SiO_2	–	23	–	–

[a] Analyzed using inductively coupled plasma technique (ICP).
[b] % ion exchange assuming that a stoichiometric exchange process take place with 4 monovalent ammonium ions being replaced by one $La(OH)^{2+}$ ion and one divalent Co^{2+} ion.
[c] Atomic ratio.
[d] Same batch of CoHM.

LaHM was also prepared. Cobalt was exchanged into LaHM, thus yielding the LaCoHM catalyst. The solids named La/HM and Co/HM were prepared by wet impregnation with the $La(NO)_3$ and $Co(CH_3COO)_2$ precursors, respectively. Before the catalytic tests all the solids were heated up in flowing O_2 at 2 °C min^{-1} to 500 °C, and kept at this temperature for 8 h (calcined catalysts). La_2O_3/SiO_2 was prepared by wet impregnation with $La(NO)_3$ and calcined up to 500 °C. It contained 27 wt% of La_2O_3 (23 wt% La). The composition of the prepared catalysts is shown in Table 1.

2.2. Catalytic test

The catalyst powders were tested in a flow, fixed-bed, quartz micro reactor. The typical composition of the dry reactant stream was the following: 1000 ppm CH_4, 1000 ppm NO and 2% O_2 in He (GHSV: 7500 h^{-1}). After the initial dry test, 10% water was added by flowing the reactant stream through a saturator. All active catalysts were kept on stream for 400 h at 500 °C under these conditions; the conversion was measured periodically. The composition of the reactor effluent was monitored for CH_4, CO, NO, N_2O and NO_2 using a Fourier-transform infrared spectrometer (FTIR), Thermo Matson Genesis II (resolution of 4 cm^{-1}) equipped with a gas IR cell, having a 15 cm path length.

The CH_4 to CO_2 and the NO_x to N_2 conversions were defined as $CNO_x = (1 - [NO_x]/[NO_x]^o) \times 100$, and $C_{CH_4} = (1 - [CH_4]/[CH_4]^o) \times 100$. $[NO_x]^o$ and $[CH_4]^o$ stand for the NO and CH_4 concentration of the feed, respectively. N_2 was measured by nitrogen balance.

2.3. X-ray diffraction (XRD)

The XRD patterns of the fresh and used solids were obtained with an XD-D1 Shimadzu instrument operated at 35 kV and 40 mA. The scan rate was 1° min^{-1} for the 2θ range of 5–50°.

2.4. Pore volume

Nitrogen adsorption isotherms were measured at 77 K in an automated Quantachrome sorptometer. The catalyst samples were outgassed at 300 °C overnight under a pressure of 10^{-3} Pa. The pore volume was calculated from the saturation N_2 adsorption capacity of the zeolite micropores.

2.5. Raman spectroscopy

The Raman spectra were recorded with a TRS-600-SZ-P Jasco Laser Raman instrument, equipped with a CCD (charge-coupled

device) with the detector cooled to about 120 °C using liquid N_2. The excitation source was the 514.5 nm line of a Spectra 9000 Photometrics Ar ion laser. The laser power was set at 30 mW (resolution 4 cm^{-1}).

2.6. Temperature-programmed reduction (H_2-TPR)

These experiments were carried out with 0.10 g of either the fresh or used catalyst with an Okhura TP-2002S instrument equipped with a TCD detector. Prior to the TPR measurements, the solids were pretreated in argon heating up to 500 °C at 2 °C min^{-1}. The reducing gas was a 5% H_2/Ar mixture which flowed at 30 cm^3 min^{-1}. The temperature was ramped up at 10 °C min^{-1} to 850 °C.

2.7. FTIR and CO adsorption

The samples were prepared by compressing the solids at 4×10^8 Pa in order to obtain self-supporting pellets. They were mounted on a transportable infrared cell with CaF_2 windows and external oven. The pretreatment was performed in a high vacuum system. The sample was first outgassed at 400 °C for 12 h in a dynamic vacuum of 1.3×10^{-4} Pa. It was then cooled to room temperature and CO was introduced into the cell controlling the CO pressure at ca. 0.13, 0.26, 0.65 and 1.46 kPa.

2.8. X-ray photoelectron spectroscopy (XPS)

XPS analyses were performed in a multi-technique system (SPECS) equipped with a dual Mg/Al X-ray source and a hemispherical PHOIBOS 150 analyzer operating in the fixed analyzer transmission (FAT) mode. The spectra were obtained with pass energy of 30 eV; the Al Kα X-ray source was operated at 100 W and 10 kV. The working pressure in the analyzing chamber was less than 5×10^{-9} mbar. The XPS analyses were performed on the calcined and used catalyst. The samples were heated up in vacuum at 400 °C in the reaction chamber of the spectrometer. The spectral regions corresponding to La 3d, Co 2p, O 1s, C 1s, Si 2p, Si 2s and Al 2p core levels were recorded for each sample. The data treatment was performed with the Casa XPS program (Casa Software Ltd., UK). The peak areas were determined by integration employing a Shirley-type background. Peaks were considered to be a mixture of Gaussian and Lorentzian functions in a 70/30 ratio. For the quantification of the elements, sensitivity factors provided by the manufacturer were used.

3. Results

3.1. Synthesized catalysts

The composition of the prepared catalysts is shown in Table 1. A new CoHM solid was prepared for each bimetallic catalyst unless otherwise indicated.

3.2. Catalytic test

To quantify the deactivation process, the catalysts were kept on stream for 400 h at 500 °C. The reactant stream contained 1000 ppm each of NO and CH_4, 2% O_2, and 10% H_2O in He. The initial NO conversion to N_2 under dry conditions was ca. 25–40% over the CoHM and the bimetallic samples, except CoLaHM-600 which was almost inactive for the SCR of NO_x with methane (initial conversion: 10%). Upon water addition the activity of the catalyst decreased but on CoLaHM-500 it increased ca. 30% (Fig. 1A). CoLaHM-500 was the best catalyst and the duplicate assay exhibited the same behavior (Fig. 1A).

The calcination temperature of the already exchanged cobalt zeolite affected the hydrothermal resistance of the catalyst. The monometallic CoHM decreased the activity from 40 to 10% (Fig. 1A). The catalytic activity of LaHM (not shown) and

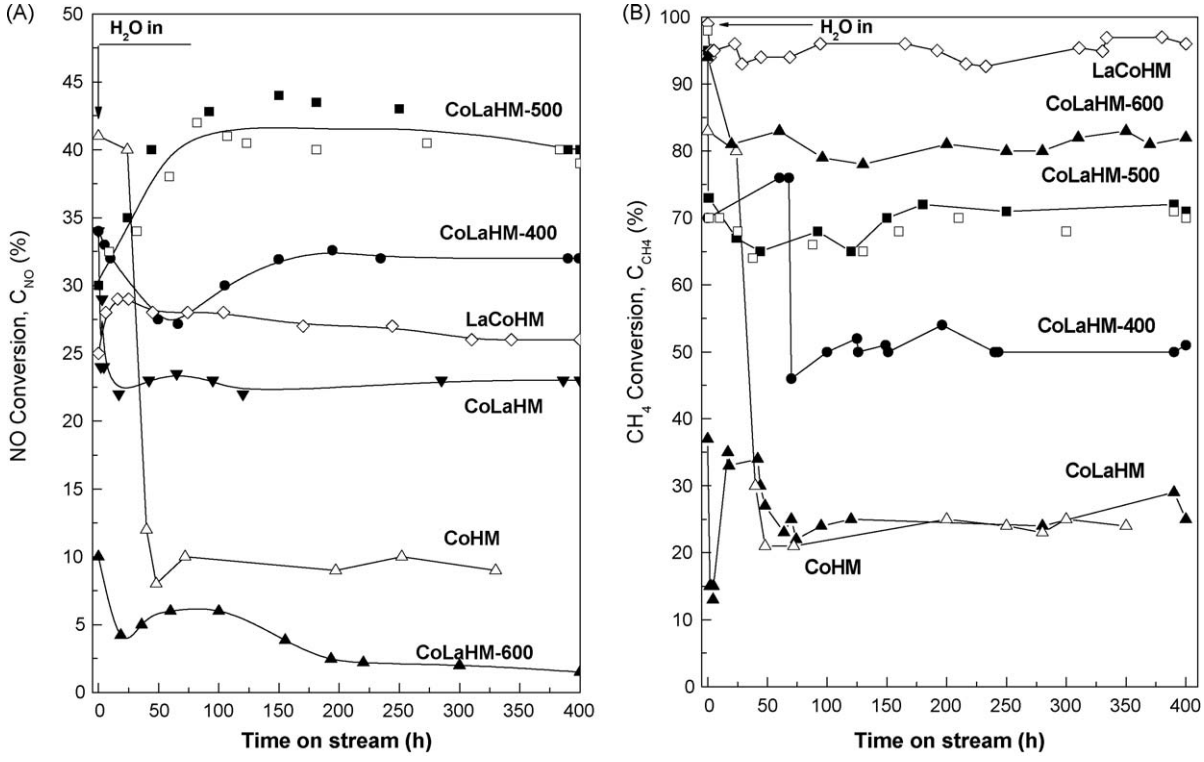

Fig. 1. Catalytic data. (A): NO to N_2 conversion. (B): CH_4 to CO_2 conversion. (■, □) CoLaHM-500 (□ second CoLaHM-500 aliquot), (•) CoLaHM-400, (◇) LaCoHM, (▼) CoLaHM, (▲) CoLaHM-600 and (△) CoHM. Reaction conditions: GHSV = 7500 h^{-1}, [NO] = [CH_4] = 1000 ppm, [O_2] = 2%, [H_2O] = 10%, T = 500 °C.

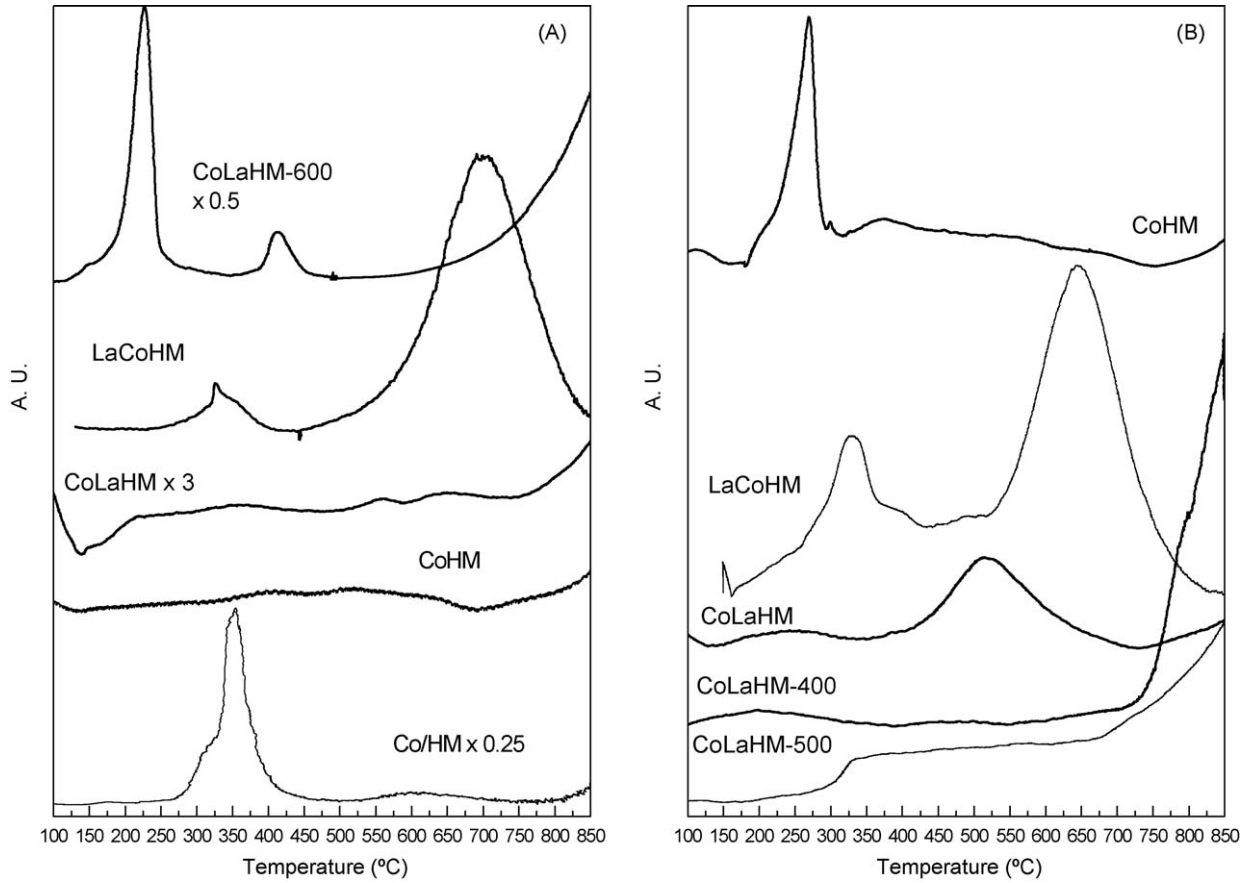

Fig. 2. TPR profiles of A: calcined catalysts and B: used catalysts. Experimental conditions: 0.1 g, 5% H_2/Ar at 30 cm^3 min^{-1}, 10 °C min^{-1}.

CoLaHM-600 resulted almost nil after 400 h on stream. Simultaneously, with the wet feed the methane conversion (Fig. 1B) decreased over all the catalysts but one (LaCoHM).

3.3. TPR

General features. TPR experiments on Co-zeolites have been extensively reported by many authors [12,14,25] who have concluded that in general the reduction profiles present three zones: ZI (100–350 °C) corresponding to cobalt oxides, ZII (350–650 °C) oxo-cations $[Co\text{-}O\text{-}Co]^{2+}$ and/or CoO_x stabilized inside the zeolite and ZIII (650–900 °C) to Co^{2+} at exchange positions.

The TPR profiles are shown in Fig. 2. The H_2 consumption ratios were calculated assuming that the cobalt not reduced at temperatures lower than 850 °C is at exchange positions (Table 2). The results show that during reaction in the CoHM catalyst, cobalt-oxide-type species (CoO_x) and/or oxo-cations $[Co\text{-}O\text{-}Co]^{2+}$ are generated inside the zeolite.

The effect of the exchange order can be seen in Fig. 2; when cobalt is exchanged before lanthanum (CoLaHM) it would locate at more coordinated positions (Co reduction temperatures higher than 800 °C). On the other hand, the presence of lanthanum in the matrix during the Co exchange (LaCoHM) would cause a cobalt fraction to be exchanged at more accessible sites (Fig. 2A) while another appears as a cobalt oxide species. On LaCoHM, the shift of the higher reduction peak towards lower temperatures after reaction would indicate that the cobalt mobility is higher than that of CoLaHM. Simultaneously, oxo-cations would be formed after reaction, most of them remaining at exchange positions (Fig. 2B). The used CoLaHM-500 catalyst presented the same reduction profile as the calcined catalyst, indicating that after reaction the cobalt species remain exchanged. The used profile of CoLaHM-400 did not show the formation of cobalt oxides species after reaction. The fresh CoLaHM-600 catalyst presented a reduction peak at 227 °C assigned to Co_3O_4 and a smaller one at 415 °C. The hydrogen consumption of these two peaks corresponds to 86% of the total cobalt load which means that only 14% cobalt remains exchanged.

3.4. Raman spectroscopy, XRD data and pore volume

Fig. 3 shows the Raman spectra of fresh and used catalysts. On the used CoHM and in both (fresh and used) CoLaHM-600, a band

Table 2
TPR. Hydrogen consumptions on calcined and used samples.

Catalyst (μmol Co)[a]	Treatment	H_2/Co[b]	
		Peak I (Tmax)	Peak II (Tmax)
Co/HM (49.32)	Calcined	0.86 (350 °C)	0.12 (615 °C)
CoHM (19.50)	Calcined	0	0
	Used	0.22 (270 °C)	0.21 (300–700)
CoLaHM (19.50)	Calcined	0	0
	Used	0	0.43 (520 °C)
LaCoHM (45.75)	Calcined	0.06 (330 °C)	0.94 (700 °C)
	Used	0.16 (330 °C)	0.86 (645 °C)
CoLaHM-500 (28.64)	Calcined	0	0[c]
	Used	0	0[c]
CoLaHM-400 (19.50)	Used	0	0[c]
CoLaHM-600 (32.71)	Calcined	0.73 (227 °C)	0.13 (415 °C)

[a] μmoles of Co per 0.1 g of sample used in the experiments.
[b] Molar ratio (μmol of H_2)/(μmol Co), peak temperatures are given between parentheses.
[c] The reduction peak begins at 750 °C.

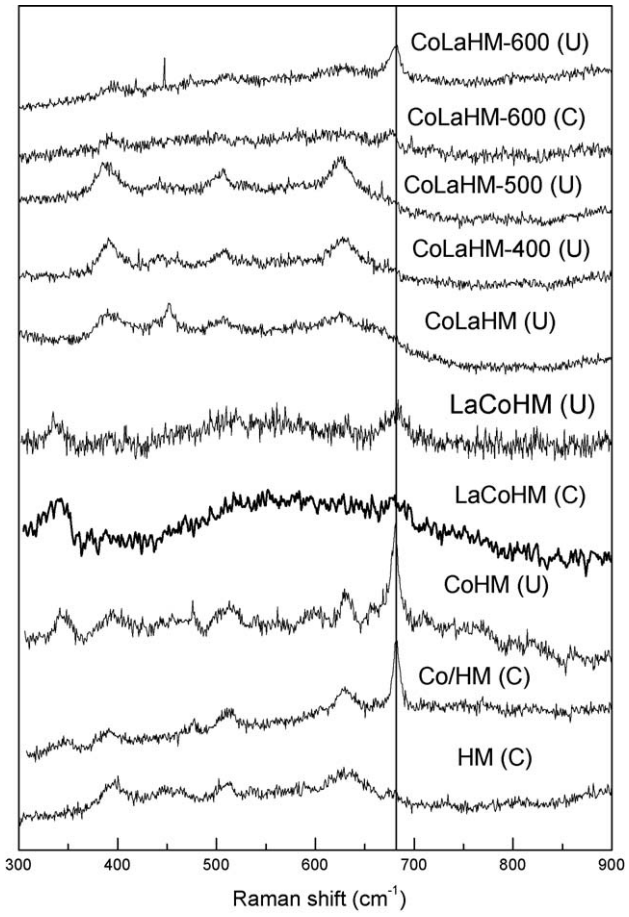

Fig. 3. Raman spectra of mono and bimetallic mordenites. (C) Calcined and (U) Used.

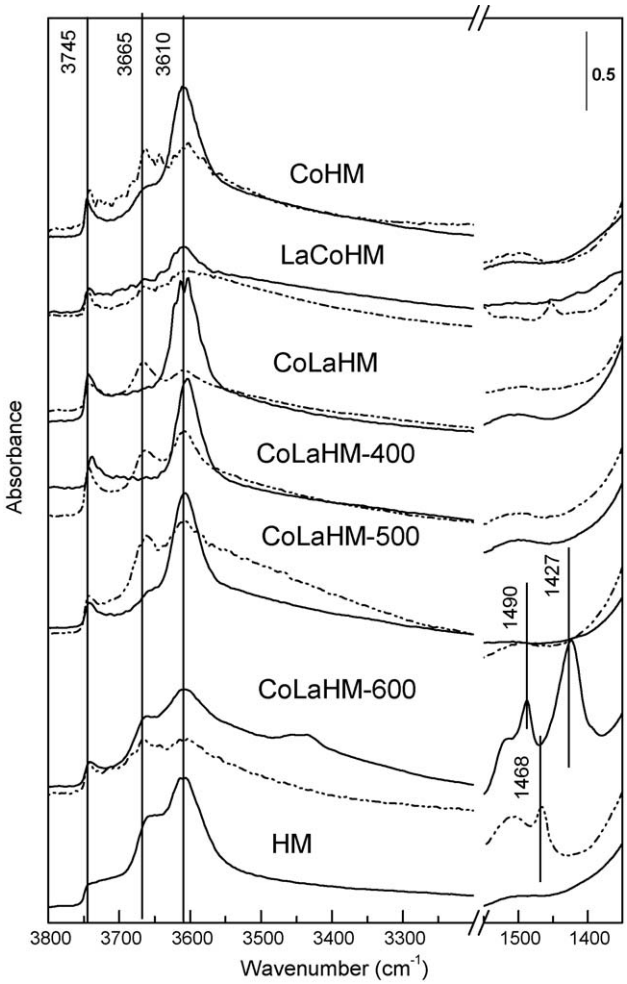

Fig. 4. IR spectra of calcined and used catalysts evacuated at 400 °C at 1.3×10^{-4} Pa before CO adsorption. Solid line: calcined. Dot line: used.

at 681 cm^{-1} is observed. This wavenumber corresponds to the strongest Raman band of Co_3O_4. The calcined catalyst prepared by the wet impregnation method (Co/HM) presents the typical signals of cobalt oxides (681, 485 cm^{-1}) and it was taken as a reference. Note that the other signals are assigned to the zeolite matrix and that there are no peaks of lanthanum compound (carbonates or $La(OH)_3$). On used LaCoHM, the main signal corresponding to Co_3O_4 is also observed, in agreement with the TPR results.

The XRD patterns of all samples are almost identical. No Co_3O_4 reflections were seen and the crystallinity of the mordenite matrix has not been altered at all by the hydrothermal treatment. This result indicates that the Co_3O_4 observed by Raman spectroscopy on CoHM and CoLaHM-600 corresponds to small particles.

No significant difference in pore volume was found among the several catalysts prepared by ionic exchange. It varied between 0.19 and 0.22 cm^3/g.

3.5. FTIR

3.5.1. IR spectra of the solids

All the catalysts were evacuated (1.3×10^{-4} Pa) at 400 °C before recording the spectra. Fig. 4 shows the spectra obtained on the used and calcined wafers before CO adsorption. The typical zeolite spectra can be observed which present: (i) The OH region (3400–3800 cm^{-1}); (ii) The TOT vibration region (2100–1570 cm^{-1}) [26] (not shown), and (iii) the carbonates and hydroxide vibrations that appear between 1400 and 1550 cm^{-1} [27,28]. Note that the CoLaHM-600 solids (calcined and used) and used LaCoHM (Fig. 4) show strong carbonate and hydroxide bands between 1400 and 1550 cm^{-1}.

The OH stretching region. The spectra show the following features (Fig. 4): (i) a band at 3610 cm^{-1} due to the OH stretching mode Si(OH)Al groups (Brönsted sites), which is somewhat asymmetric due to the OH bond heterogeneity. This band is characterized by a tail towards lower frequencies, due to the bridging OHs located in the so-called side pockets, (ii) a band at 3665 cm^{-1}, which is small on the fresh solids but whose intensity increases after reaction. This band could be associated with either $(Co\text{-}OH)^+$ species at exchange positions [8] or extraframework aluminum (EFAl) [29,30]. At framework positions, the aluminum is usually tetrahedrally coordinated with 4 oxygen atoms and upon dehydroxylation, some of this aluminum becomes tricoordinated and forms Lewis acid sites, and (iii) a peak centered at 3745 cm^{-1} assigned to the O–H stretching vibrations of free silanol groups (i.e., silanols that are not interacting through hydrogen bonding because they are isolated or at terminal positions), and silica or amorphous silica–alumina SiOH groups.

The mono and bimetallic Co-exchanged mordenite (CoHM) and HM samples show the same bands that seem not to be affected by the ion exchange process. The band at 3665 cm^{-1} increases in all the catalysts after reaction and the greatest increase is observed in CoHM. In the CoLaHM-400 and CoLaHM-500 samples, the increase is not due to the presence of $(Co\text{-}OH)^+$ since these entities were not observed in the TPR profiles; instead, it could be due to the formation of EFAl or some La^{+3} species.

In all the spectra, the band at 3745 cm^{-1} corresponding to silanol groups was fitted considering a 100% Lorenzian function

Table 3
Integrated absorbance ratios.

Catalyst	Treatment	I_{3745}/I_T[a]
CoHM	Calcined	0.03
	Used	0.06
LaCoHM	Calcined	0.04
	Used	0.04
CoLaHM	Calcined	0.06
	Used	0.06
CoLaHM-400	Calcined	0.06
	Used	0.06
CoLaHM-500	Calcined	0.04
	Used	0.04
CoLaHM-600	Calcined	0.04
	Used	0.06
LaHM	Calcined	0.04
	Used	0.04

[a] I_T: Total integrated area between 3300 and 3800 cm^{-1}.

with a FWHM = 15 cm^{-1} and the integrated areas were related to the total area in the 3300–3800 cm^{-1} range (Table 3). Only in the CoHM and CoLaHM-600 catalysts, was a significant increment of this ratio observed after reaction. This is consistent with a certain extent of lattice destruction during reaction.

3.5.2. CO adsorption

The investigation of the oxidation state of the metal species on surfaces may conveniently be carried out by the monitoring of CO adsorption by FTIR.

3.5.2.1. Support, HM. Fig. 5A shows the spectra of CO adsorbed on the parent HM. The band at 2167 cm^{-1} is due to CO interacting with the Brönsted acidic bridging hydroxyls and it is the most intense band at high CO pressure, whereas the band at 2140 cm^{-1} is due to weakly bonded physisorbed CO [31]. The bands at 2220 and 2194 cm^{-1} are assigned to CO interacting with acidic Al^{+3} centers.

Aluminum ions at framework positions of defect-free zeolites do not adsorb CO, even at low temperature. In agreement with our results, EFAl sites were shown to be present in ZSM-5 and Y-zeolites by a carbonyl band at 2227–2225 cm^{-1} and in HM by bands at 2218–2220 cm^{-1} [32,33].

3.5.2.2. Monometallic samples. The catalyst prepared by wet impregnation in which the cation should have mainly an oxide behavior was taken as reference. Fig. 5B and C show the CO adsorption spectra of La/HM and Co/HM.

La/HM. Note that both this sample and the HM support exhibit very weak CO adsorption capacity (Fig. 5A and B). Comparing both spectra, a new band appears in the La/HM spectrum at 2184 cm^{-1} assigned to La^{+3} at exchange positions, probably forming La-OH species ($La(OH)^{2+}$, $La(OH)_2^{+}$). The presence of lanthanum at exchange positions can be due to the migration of hydrolyzed lanthanum species such as $La(OH)^{2+}$ into the matrix during the La/HM preparation and during the calcination treatment. The bands associated with Lewis acid sites (2220 and 2194 cm^{-1}) are very weak, probably because the La oxide supported on the zeolite has covered these species and CO cannot be adsorbed. The presence of CO adsorption at room temperature on La_2O_3 leads to the formation of carbonate and carbonite structures but not to carbonyl complexes [32]. We checked that CO does not adsorb on lanthanum oxide (La_2O_3) by monitoring the CO adsorption (not shown) on a sample prepared by wet impregnation of $La(NO)_3$ on SiO_2 (La_2O_3/ SiO_2).

Co/HM. The CO adsorption spectra (Fig. 5C) show two well-defined bands, at 2205 and 2160 cm^{-1}, respectively, which correspond to adsorbed CO on Co^{2+} at exchange positions [34] and Co_3O_4 [29] respectively. This result agrees with the Raman spectra where the Co_3O_4 fingerprint is present. Again, during the impregnation, some cobalt migrates into the matrix and remains associated with the oxo-cobalt species. Note that this solid adsorbs larger amounts of CO than the two previous preparations (Fig. 5A and B).

LaHM. The adsorption of CO at RT on fresh LaHM (Fig. 6A) shows a strong band at 2189 cm^{-1} associated with La at exchange positions. At higher CO pressure a shoulder appears at 2173 cm^{-1}, suggesting that there is a less accessible La adsorption site in the matrix. A weak CO-EFAl signal also appears at 2220 cm^{-1}. On the used catalyst (Fig. 6B), the main band that can be observed is at 2182 cm^{-1} meaning that some change on the coordination state of

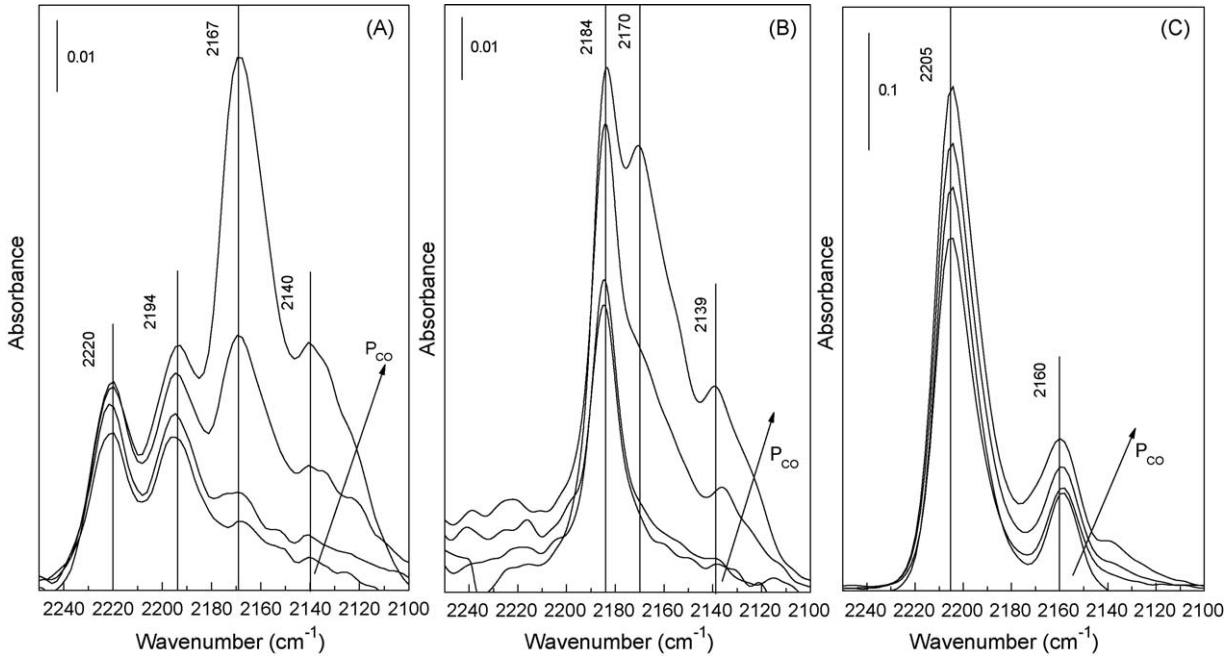

Fig. 5. FTIR spectra of CO adsorbed on calcined samples: (A): HM, (B): La/HM and (C): Co/HM. P_{CO}: 0.13, 0.26, 0.65 and 1.46 kPa.

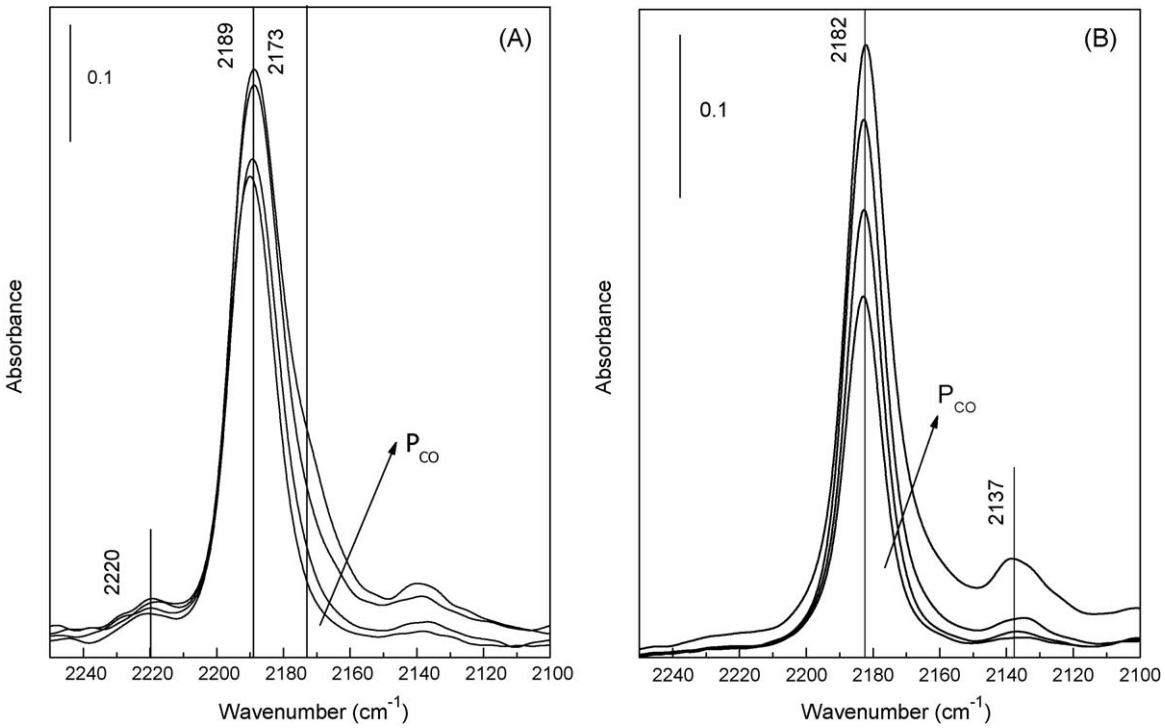

Fig. 6. FTIR spectra of CO adsorbed on LaHM. (A): Calcined and (B): Used. P_{CO}: 0.13, 0.26, 0.65 and 1.46 kPa.

the rare-earth, or migration to other sites, occurred. The frequency of this band does not change with the CO pressure (from 0.13 to 1.46 kPa), indicating that CO adsorbed on isolated La sites.

CoHM. In Fig. 7A and B the CO adsorption spectra obtained on fresh and used CoHM are reported. The main band corresponds to cobalt at exchange positions; in both cases the cobalt species are well dispersed as there is no shift when the CO pressure is increased. After reaction, the spectra bandwidth is lower; some reorganization of the cobalt species may have occurred. A contribution of CO adsorbed on cobalt oxide also appears at 2159 cm^{-1}. The deconvolution (not shown) of the calcined sample shows the presence of two Co-exchanged bands: β sites at 2191 cm^{-1} and α site at 2206 cm^{-1}. The band at 2170 cm^{-1} at high CO pressure (Fig. 7A) confirms the presence of remaining Brönsted sites from the HM. The Co_α/Co_β (I(2206)/I(2191)) ratio increases considerably after reaction, suggesting that the presence of Co

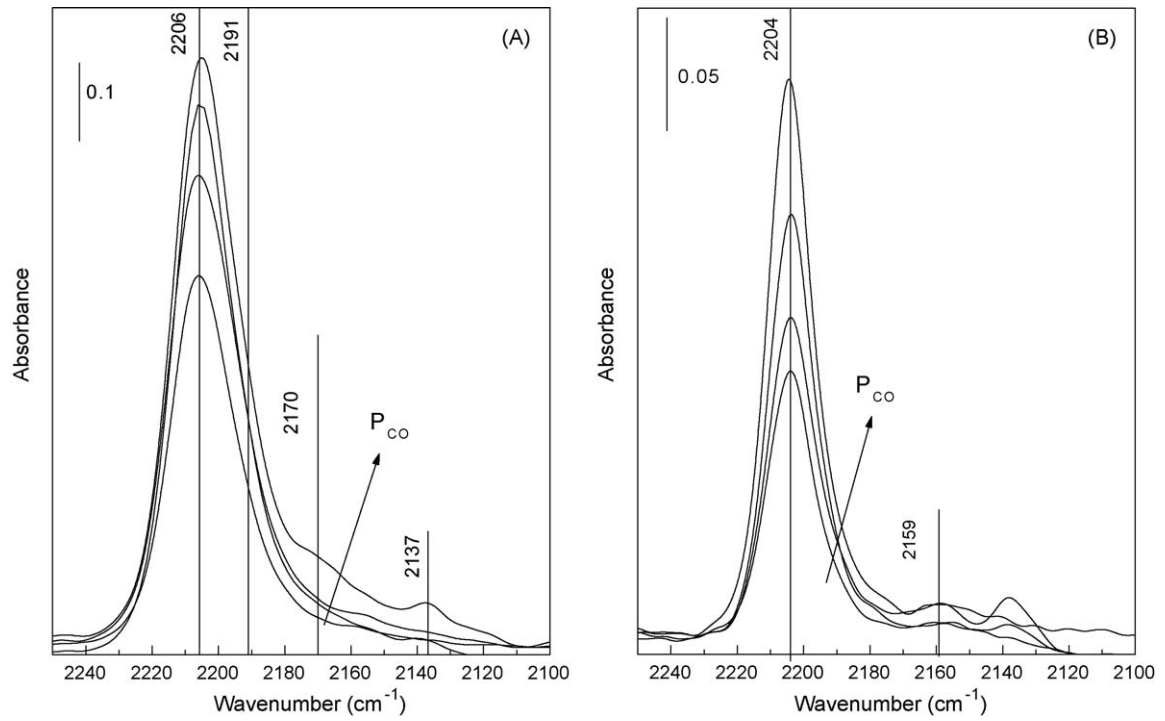

Fig. 7. FTIR spectra of CO adsorbed on CoHM. (A): Calcined and (B): Used. P_{CO}: 0.13, 0.26, 0.65 and 1.46 kPa.

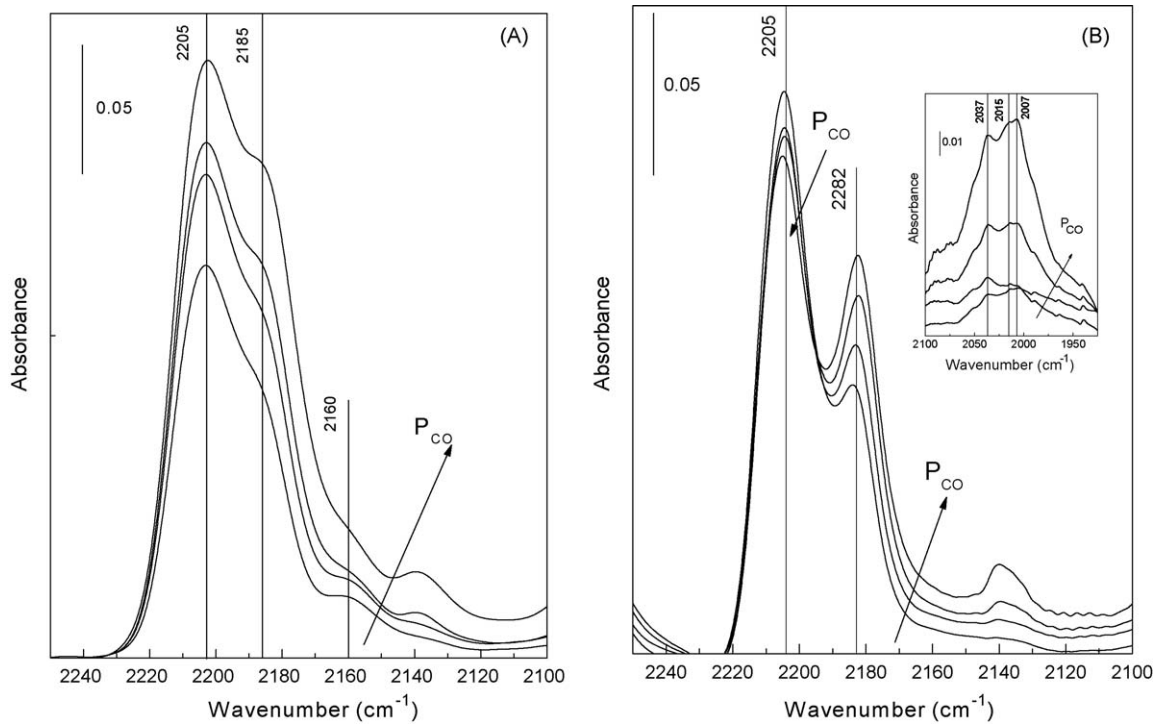

Fig. 8. FTIR spectra of CO adsorbed on LaCoHM. (A): Calcined and (B): Used. P_{CO}: 0.13, 0.26, 0.65 and 1.46 kPa.

oxides interferes with Co_{β} adsorption centers. Note that the intensities of the bands are lower and more sensitive to pressure than in the fresh solid. This could suggest that cobalt adsorption sites have decreased because of the formation of cobalt oxide which partially blocks the zeolite channels and/or because of the partial destruction of the mordenite structure.

3.5.2.3. Bimetallic samples. LaCoHM. An adsorption band at 2205 cm^{-1} corresponding to Co^{2+} at exchange positions is observed, partially overlapping with the signal at 2185 cm^{-1} corresponding to the CO adsorption on exchanged lanthanum (Fig. 8A). These bands are better defined and remain at the same position after reaction (Fig. 8B).

On the used catalyst (Fig. 8B) a singular situation aroused: the adsorption band corresponding to CO-Co^{+2} decreased when the CO pressure increased, and a new band appeared in the 2050–2000 region (inside Fig. 8B) corresponding to the linear form of CO adsorbed on cobalt metal sites (CO-Co^{0}) [35]. This can be explained

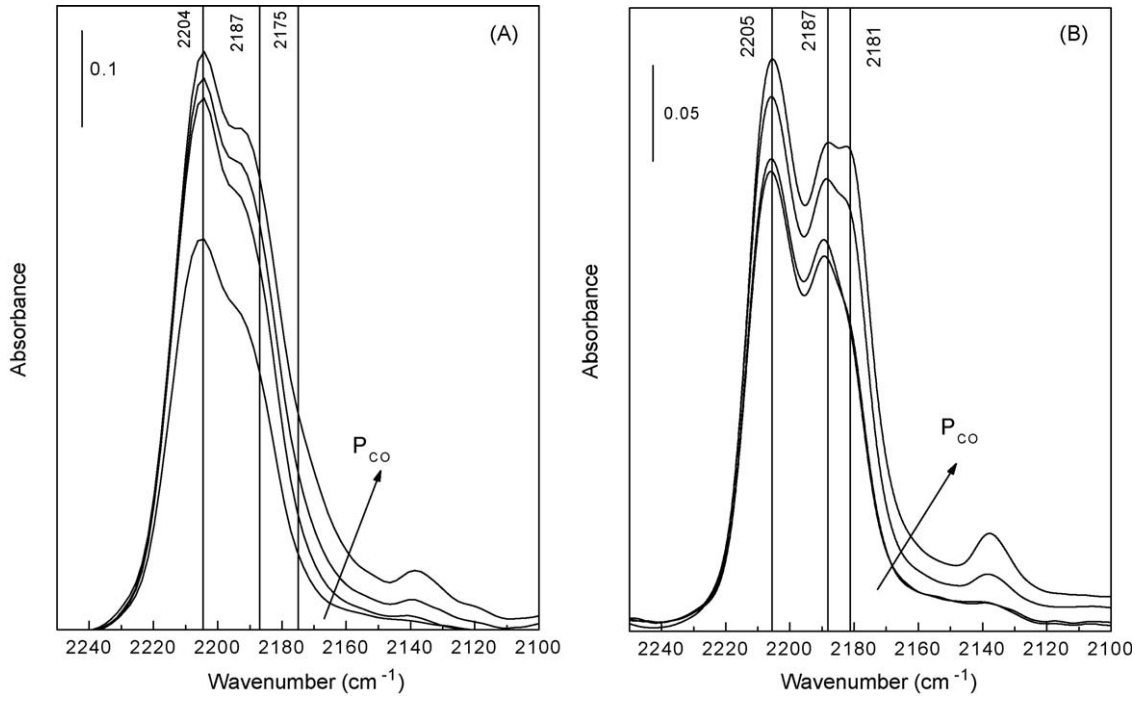

Fig. 9. FTIR spectra of CO adsorbed on CoLaHM. (A): Calcined and (B): Used. P_{CO}: 0.13, 0.26, 0.65 and 1.46 kPa.

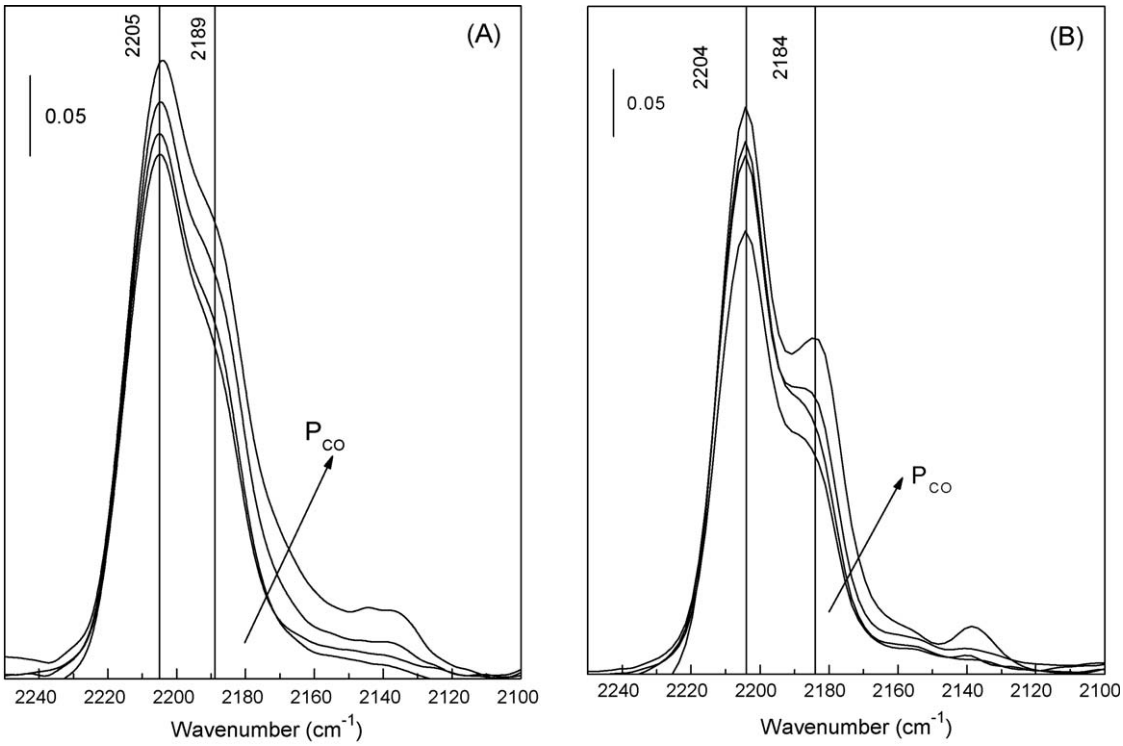

Fig. 10. FTIR spectra of CO adsorbed on CoLaHM-400. (A): Calcined and (B): Used. P_{CO}: 0.13, 0.26, 0.65 and 1.46 kPa.

by the reduction of cobalt oxide particles supported on the zeolite surface during CO adsorption. Note that this is the only sample where Co was exchanged after La. In this vein, only the calcined spectra showed CO adsorption on the Co oxide band (2160 cm^{-1}). The presence of these oxides while on stream could also explain that this catalyst shows the highest CH_4 conversion to CO_2 (Fig. 1B).

CoLaHM. Fig. 9A shows that on the calcined solid, the CO adsorption band on Co^{2+} at exchange positions is observed together with the not well-defined band at 2187 cm^{-1} corresponding to CO interacting with lanthanum at exchange positions (see also Fig. 6). No band shifts occurred upon the CO pressure increase.

In the wide band of the CO adsorbed on the calcined sample, the contributions of two bands can be sorted out: at 2187 and at 2175 cm^{-1}, similar to those observed on LaHM (Fig. 6A). After reaction, the CO adsorption bands corresponding to Co and La are better defined (Fig. 9B).

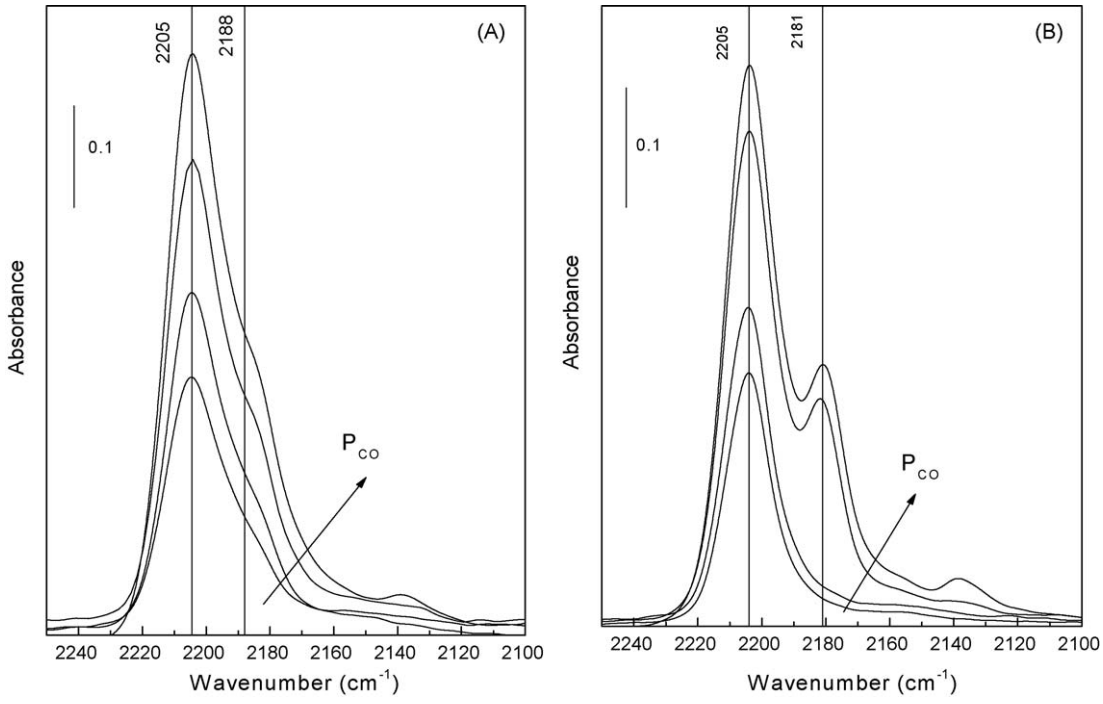

Fig. 11. FTIR spectra of CO adsorbed on CoLaHM-500. (A): Calcined and (B): Used. P_{CO}: 0.13, 0.26, 0.65 and 1.46 kPa.

This is the only case where two bands are seen for the CO interaction with La. The one at 2187 cm^{-1} appears at the same frequency observed in all the fresh catalysts while the second one at 2181 cm^{-1} is characteristic of all the used catalysts.

CoLaHM-400. CO adsorbed species on Co^{2+} are identified by the band at 2205 Fig. 10A and B. A shoulder at 2189 cm^{-1} is indicative of the presence of La at exchange positions. Again after use, CO-Co^{2+} becomes narrower and the CO-La band shifts to 2184 cm^{-1}. Note that the intensity ratio of the two bands is now higher than in CoLaHM.

CoLaHM-500. The calcined sample shows a less intense shoulder than those of the previous samples (Fig. 11A). On the used catalyst the CO adsorption band on lanthanum species appears at lower frequency (2181 cm^{-1}) and it is not observed until higher P_{CO} (Fig. 11B).

CoLaHM-600. The spectra obtained on both used and calcined samples are very similar. The main band observed is CO adsorbed on cobalt at exchange positions and a tail centered at 2186 cm^{-1} assigned to the lanthanum species (Fig. 12A and B). This result agrees with the FTIR spectra which show the presence of hydroxyl and carbonated La species which do not adsorb CO (Fig. 4). A contribution of the adsorbed band of CO on cobalt oxide can also be observed in agreement with Raman results (Fig. 3). Note that although cobalt oxides are present, the adsorption intensity does not change. This suggests that in this case the formation of cobalt oxide does not block the zeolitic channels.

3.6. XPS results

The Co^{2+} and Co^{3+} oxidation states can be distinguished by the presence of a distinct shake-up satellite structure in the Co 2p spectra. The high spin Co^{2+} compounds have intense satellite bands, arising from the presence of unpaired electrons in their valence orbital. Co^{3+} oxides exhibit only a very weak satellite band in their Co 2p spectra. No satellite peaks in the XPS profile would be indicative of complete oxidation of Co^{2+} to Co^{3+}.

On examining the XPS profile of the La-Co-exchanged catalyst, the existence of Co^{2+} has been confirmed (Table 4 and Fig. 13A). The Co 2p satellite intensities approach satellite/main peak intensity ratios observed for bulk CoO, while the strong satellite lines are centered about 4.2–4.7 eV above the principal line. These observations indicate that the surface Co^{2+} species are not being oxidized to Co^{3+} after calcination.

The high BEs (ca. 782.7 eV) of CoLaHM and CoLaHM-500 might be related to strong interactions between cobalt and other atoms of the solid matrix and/or to highly dispersed cobalt. Similar binding energies were reported [9,36] for the ion exchanged form of cobalt in ZSM-5 and PtCo-zeolites. In those solids, the high-binding energy values are suggestive of cobalt in a highly oxidizing environment.

However, the LaCoHM and CoLaHM-600 catalysts show a Co $2p_{3/2}$ BE value close to 781.3 eV, suggesting the presence of Co(II) (tetrahedral) reported on Co/SiO_2 supported catalysts [37] in agreement with the TPR, Raman and CO adsorption results (Table 2, Figs. 8 and 12).

Fig. 13B shows the typical La $3d_{5/2}$ spectrum observed from $La_2O_2CO_3$ samples calcined at 550 °C. The La 3d doublet was well-defined. The satellites appearing on the high side of $3d_{5/2}$ and $3d_{3/2}$ peaks result from competitive core-hole screening by the nearly degenerate ligand 2p and empty La 4f orbital [38]. The binding energy and peak width are shown in Table 4. The La $3d_{5/2}$ core level is observed at 835 eV and the corresponding satellite-split is 3.7 eV. These values agree well with those previously reported by Gallaher et al. [39] for La_2O_3.

Fig. 13B also compares the La 3d spectra for La-exchanged zeolites. The binding energy values range between 836 and 837 eV. All samples exhibit a broad La $3d_{5/2}$ satellite (FWHM greater than 3.0 eV). However, the satellite/ main peak intensity ratios (Table 4) were slightly higher than the value observed in the lanthanum oxide sample calcined at 550 °C (0.77).

Similar binding energies were previously reported by Karge and co-workers [40]. They sustained that there was no reason to assume that the oxidation state of La should deviate from +3 in

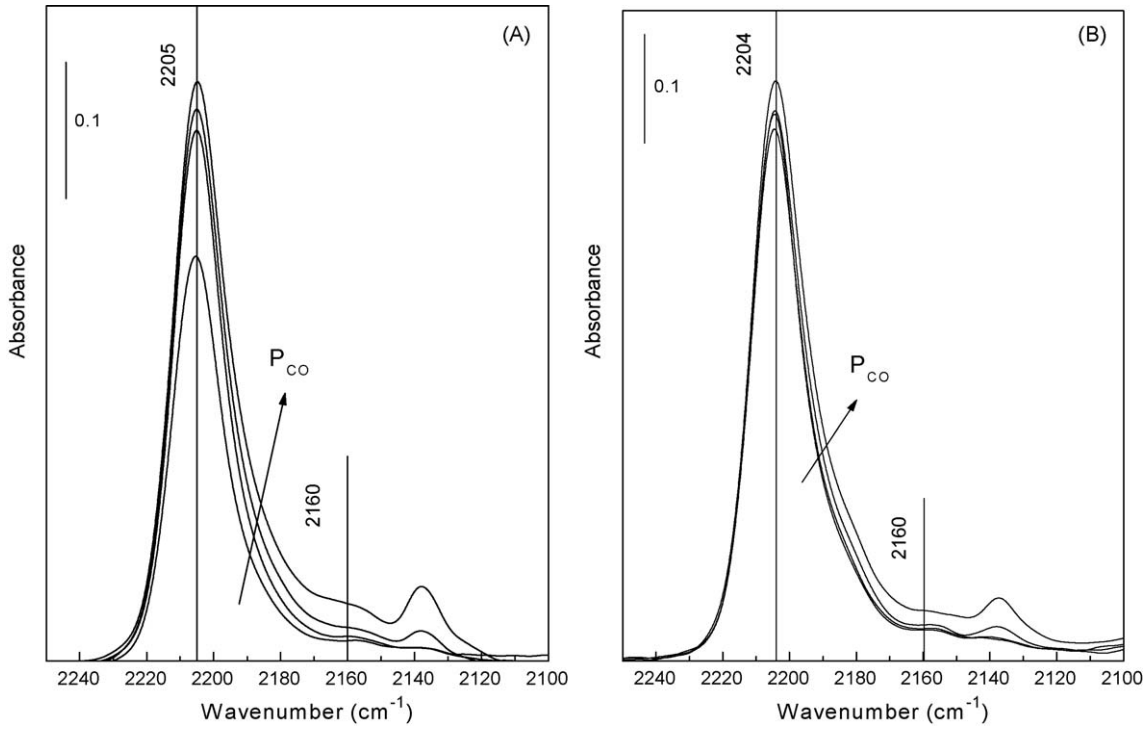

Fig. 12. FTIR spectra of CO adsorbed on CoLaHM-600. (A): Calcined and (B): Used. P_{CO}: 0.13, 0.26, 0.65 and 1.46 kPa.

Table 4
XPS data[a].

Solids	Co $2p_{3/2}$[b]	Co $2p_{3/2}$[b] Satellite	Isat/IMP_{Co}[c]	La $3d_{5/2}$[b]	La $3d_{5/2}$[b] Satellite	Isat/IMP_{La}[d]	%Co[e]	%La[e]
$La_2O_2CO_3$	–	–	–	835.0(3.1)	838.7(2.9)	0.77	–	–
CoO[f]	780.5	786.9	0.90	–	–	–	–	–
	780.1	788.0	–					
Co_3O_4[f]	779.5	788.0	–	–	–	–	–	–
	779.6	787.1	–					
$Co(OH)_2$[f]	781.0	786.4	–	–	–	–	–	–
LaHM	–	–	–	836.4(3.0)	839.8(3.6)	0.91	–	–
LaCoHM	781.4(3.9)	786.4(5.8)	0.78	836.0(3.0)	839.8(3.3)	1.33	5.60	0.39
CoLaHM	–	–		836.6(3.0)	840.0(3.4)	0.83	0.19	0.35
Used	782.5(3.4)	787.1(5.5)	1.00	836.2(3.0)	839.5(3.8)	1.00	0.37	0.29
CoLaHM-500	782.9(3.6)	787.4(5.3)	0.67	837.0(2.8)	840.5(3.2)	0.83	0.60	0.23
Used	782.3(3.3)	786.7(6.2)	0.86	836.2(3.4)	839.7(3.7)	1.00	0.96	0.51
CoLaHM-600	781.3(3.6)	786.0(7.0)	1.20	835.6(3.3)	839.1(3.6)	0.83	2.20	0.90
Used	781.6(3.5)	786.0(6.8)	1.20	835.8(3.3)	839.3(3.4)	0.83	1.67	0.59

[a] For all samples, the binding energies of Al, Si, O and C were the following: C 1s = 284.8 eV, Al 2p = 74.1 eV, Si 2p = 102.6 ± 0.1 eV, O 1s = 531.9 ± 0.1 eV.
[b] FWHM (eV) are shown between parenthesis.
[c] Intensity ratio shake-up satellite/main peak for Co $2p_{3/2}$
[d] Intensity ratio shake-up satellite/main peak for La $3d_{5/2}$.
[e] XPS surface atomic concentration.
[f] Reference [37].

the zeolite samples. Then, the binding energies reflected the difference in the chemical environment of the La ions. They suggested that in the case of the rare-earth elements, La, a significant contribution to the BE shift between the ions in the bulk oxide and the zeolite environment should originate from the same final-state effects that dominate the photoemission of the rare-earth atoms. The relevant difference between the two environments is the lower periodicity of the zeolite oxygen lattice, which is disturbed by the random distribution of the Si and Al ions, by their different covalent bonding contributions, and by the influence of cations (La^{3+}, Na^+, H^+) at specific cation sites. The BE difference between La(3d) in La_2O_3 and in La zeolites was assigned to La ions highly dispersed in the zeolite lattice. The authors compared the La signal shapes of La_2O_3 and of La zeolites, and attributed the decreased contribution of the high-BE La component in the zeolites to the fact that the La ions are coordinated by H_2O molecules and by oxygen engaged in the partially covalent bonding of the zeolite framework.

In the CoLaHM-600 sample, the La $3d_{5/2}$ BE was equal to 835.6 eV. This low-value is in agreement with the FTIR and CO

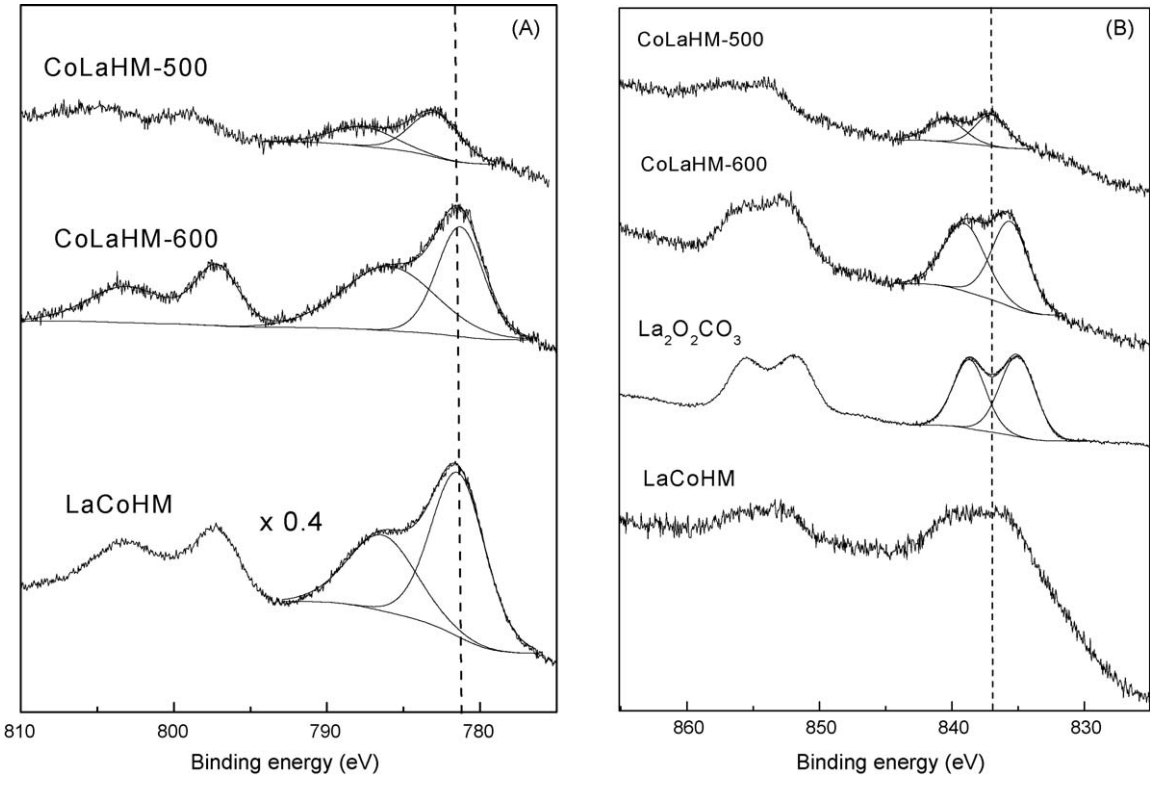

Fig. 13. XPS spectra of fresh and used catalysts. (A): Co 2p region and (B): La 3d region.

adsorption results, in which bands assigned to carbonated and hydroxyl species were observed.

In agreement with TPR (Table 2, Fig. 2) and Raman (Fig. 3) data, a high surface Co concentration is present in the LaCoHM and CoLaHM-600 (Table 4). On the other hand, the CoLaHM and CoLaHM-500 samples which only contain Co^{+2}-exchanged species show low surface Co concentrations.

4. Discussion

The appearance of cobalt oxides and the migration of Co^{2+} to less accessible sites are the main factors affecting the selectivity and activity of cobalt-containing formulations. During reaction, the exchanged Co^{2+} may suffer different transformations such as reordering and segregation under the form of oxides which lead to the loss of active species and/or to the modification of the structure [8,24]. The latter generates the loss of network aluminum and the consequent partial deterioration of the structure. The formation of cobalt oxides favors the oxidation of the hydrocarbon, thus decreasing the catalyst selectivity to the NO reduction reaction [41]. Thus, in order to attain a stable catalyst under severe hydrothermal conditions, it is essential that cobalt remains at exchange positions during reaction, preventing the formation of oxides.

In this work, after 50 h on stream, the CoHM catalyst lost almost all of its activity (Fig. 1). The characterization of this catalyst, fresh and used, showed that after reaction cobalt oxide was formed and some mobilization of exchanged cobalt occurred (Figs. 2, 3 and 7). The lower intensity of the CO adsorption band on the used solid might be symptomatic of the partial blockage of the zeolitic channels which may lead to the loss of active sites for NO_x reduction. CO adsorption data also suggest that the cobalt species in β positions have migrated towards different lattice positions or that these sites have been blocked by the cobalt oxides formed during reaction or by a partial destruction of the matrix (Table 3) or a combination of these factors.

After more than 50 h on stream, the exchange order of lanthanum and cobalt did not affect the conversion of NO_x to N_2 significantly (Fig. 1A). The slightly higher activity of LaCoHM could be attributed to its higher cobalt loading. However, a great difference was observed in the oxidation of methane to CO_2 (Fig. 1B). This behavior could be associated with the presence of cobalt oxides in LaCoHM observed by Raman, TPR and XPS (Figs. 2 and 3 and Tables 2 and 4). The XPS analyses of the catalyst indicate that the surface Co concentration is unusually high (5.60%). Furthermore, the Co 2p BE shifts to lower values, consistent with the coexistence of surface cobalt oxide (Table 4). On the other hand, in CoLaHM it becomes evident that no surface cobalt oxides are seen through XPS as the %Co is now low (0.37 vs 5.60) and the Co 2p BE exactly coincides with cobalt-exchanged mordenite.

The CO adsorption data further confirm the picture delineated by the XPS data. Fig. 8 shows that the CO-Co_xO_y signal almost disappears, while a CO-Co^0 band appears in the used catalyst. This indicates that these active oxides can be reduced by CO at room temperature. This is the only case among the catalysts studied in which this reduction occurred. Thus, when cobalt is exchanged after La, a portion of the former stays on the surface and another portion is exchanged at low coordinated sites, both being easily oxidized on stream.

The optimum calcination temperature of CoHM (before La exchange) to achieve the highest NO_x to N_2 conversion was 500 °C (Fig. 1A). Increasing the calcination temperature from ambient to 500 °C produced an increase of the CO-Co^{2+}/CO-La intensity ratio (Figs. 9–11). Note that after calcination at 500 °C (Fig. 11), the exchanged La moved to less accessible positions for in the used catalyst the CO-La band is not seen at the lower CO pressures (Fig. 11B). Then, it seems that in this case, since La has penetrated deeper in the mordenite lattice, it has less interaction with the exchanged Co^{2+} which fully develops its ability to selectively reduce NO_x to N_2. This overall picture is supported by the TPR, Raman and XPS data that show that Co^{2+} remains at exchange positions after 400 h on stream.

The stable lanthanum containing catalysts show a long stabilization period (up to 150 h) during which the NO to N_2 conversion is not constant (Fig. 1A). This behavior could be related to the reordering of the cobalt species in lattice positions of different coordination and accessibility (e.g. Co_α and Co_β). This process seems to be deeply affected by the calcination temperature of the Co-exchanged mordenite. The calcination at 500 °C yields the best catalyst, probably due to a higher exposure of the exchanged Co^{2+} ions to the reactants. This tentative explanation is inspired in the studies reported by Wichterlová and co-workers [42,43]. They thoroughly investigated the location of exchange sites in the mordenite structure and the migration of cobalt affected by the exposure to different atmospheres and temperatures. Along these lines, Gutierrez et al. [24] studied the deactivation of CoHM and PtCoHM. They assigned the rapid deactivation of these catalysts to the migration of Co^{2+} to less accessible positions in the zeolite framework.

When the CoHM solid was calcined at 600 °C before the lanthanum exchange, a catalyst was obtained with a high proportion of cobalt oxide (Figs. 2, 3 and 12 and Table 4); hence, the very low activity of CoLaHM-600 for NO_x reduction and the high activity for methane oxidation. Besides, it is observed that La is partially located outside the network as shown by the appearance of typical bands of carbonate and lanthanum oxide (Fig. 4), species that do not adsorb CO.

In the stable catalysts (LaCoHM, CoLaHM, CoLaHM-400 and CoLaHM-500), La is invariably located at exchange positions even after 400 h on stream. This is supported by the CO-La adsorption band and the constancy of La $3d_{5/2}$ BE. This is not the case of CoLaHM-600 which does not adsorb CO and shows carbonate FTIR bands.

5. Conclusions

The addition of lanthanum significantly increased the hydrothermal stability of CoHM. No change in catalytic activity for the SCR of NO_x with CH_4 occurred after 400 h on stream at 500 °C in the presence of 10% H_2O. The most active catalyst was obtained by firstly exchanging Co, then calcining the solid at 500 °C, and finally exchanging La. In these cases, the instrumental techniques used in these studies evidenced that the La cations remained at exchange positions after use. On the other hand, when La was either absent (CoHM) or had partly migrated out of the exchange positions, cobalt oxides rapidly formed (CoLaHM-600), in this way negatively affecting the selectivity towards N_2 production.

The calcination of CoHM at different temperatures before La exchange seems to modify the Co^{2+} distribution among the exchange sites of the mordenite lattice. This in turn affects the location of the $La(OH)^{2+}$ cations entering the zeolite network.

In brief, the presence of La at exchange positions seems to minimize the generation of segregated cobalt oxides and matrix dealumination. These two processes are intrinsically connected.

Acknowledgments

The authors wish to acknowledge the financial support received from UNL, CONICET and ANPCyT. They are also grateful to the Japan International Cooperation Agency (JICA) for the donation of some of the instruments used in this study. Thanks are given to ANPCyT

for Grant PME 8–2003 to purchase the UHV Multi-technique Surface Analysis System.

Thanks are also given to Elsa Grimaldi for the English language editing, to Leticia Gómez and Cecilia Pérez for their help with the catalytic activity experiments and to Claudio Maitre for technical assistance.

Finally, our special gratitude to Prof. Laura Cornaglia for the XPS measurements and for her invaluable help in the discussion of the results.

References

[1] W. Held, A. Koning, T. Richte, W. Puppe, SAE Technical Paper 900496 (1990).
[2] M.I. Iwamoto, H. Yahiro, S.Yu. Shundo, N. Mizuno, Sakubai (Catalysts) 33 (1990) 430.
[3] J.N. Armor, Catal. Today 26 (1995) 147.
[4] P. Budi, R.F. Howe, Catal. Today 38 (1997) 175.
[5] J.A.Z. Pieterse, R.W. Van den Brink, S. Booneveled, F.A. De Bruijin, Appl. Catal. B: Environ. 46 (2003) 239.
[6] A. Boix, E.E. Miró, E.A. Lombardo, M.A. Bañares, R. Mariscal, J.L.G. Fierro, J. Catal. 217 (2003) 186.
[7] P. Praserthdam, N. Mongkolsiri, P. Kanchanawanchkun, Catal. Commun. 3 (2002) 191.
[8] M.A. Ulla, L. Gutierrez, E.A. Lombardo, F. Lónyi, J. Valyon, Appl. Catal. A: Gen. 277 (2004) 227.
[9] L. Gutierrez, A. Boix, E.A. Lombardo, J.L.G. Fierro, J. Catal. 199 (2001) 60.
[10] M. Ogura, S. Koge, M. Hayashi, M. Matsukata, E. Kikuchi, Appl. Catal. B: Environ. (2000) L213.
[11] F. Bustamante, F. Córdoba, M. Yates, C. Montes, Appl. Catal. A: Gen. 234 (2002) 127.
[12] L. Gutierrez, A. Boix, J.O. Petunchi, J. Catal. 179 (1998) 179.
[13] L. Gutierrez, A. Boix, J.O. Petunchi, Catal. Today 54 (1999) 451.
[14] Luis Fernando Córdoba, Gustavo A. Fuentes, Consuelo Montes de Correa, Microporous Mesoporous Mater. 77 (2005) 193.
[15] Eduardo Falabella Sousa-Aguiar, Vera Lúcia Doria Camorim, Fatima Maria Zanon Zotin, Ronaldo Luiz Correa dos Santos, Microporous Mesoporous Mater. 25 (1998) 25.
[16] J.R. Bartlett, R.P. Cooney, R.A. Kydd, J. Catal. 114 (1988) 53.
[17] J.G. Kim, T. Kompany, R. Ryoo, T. Ito, J. Fraissard, Zeolites 14 (1994) 427.
[18] J.G. Nery, Y.P. Mascarenhas, T.J. Bonagamba, N.C. Mello, E. Falabella, S. Aguiar, Zeolites 18 (1997) 44.
[19] E.F.T. Lee, L.V.C. Rees, Zeolites 7 (1987) 446.
[20] R. Carvajal, P. Chee, J.H. Lunsford, J. Catal. 125 (1990) 123.
[21] F. Lemos, F.R. Ribeiro, M. Kern, G. Giannetto, M. Guisnet, Appl. Catal. 39 (1988) 227.
[22] Gang Yang, Yan Wang, Danhong Zhou, Jianqin Zhuang, Xianchun Liu, Xiuwen Han, Xinhe Bao, J. Chem. Phys. 119 (18) (2003) 9765.
[23] Gang Yang, Jianqin Zhuang, Yan Wang, Danhong Zhou, Maoqing Yang, Xianchun Liu, Xiuwen Han, Xinhe Bao, J. Mol. Struct. 737 (2005) 271.
[24] L. Gutierrez, M.A. Ulla, E.A. Lombardo, A. Kovács, F. Lónyi, J. Valyon, Appl. Catal A: Gen. 292 (2005) 154.
[25] Xiang Wang, Hai Ying Chen, W.N.H. Sachtler, Appl. Catal. B: Environ. 26 (2000) L227.
[26] D.W. Breck, Zeolite Molecular Sieves, John Wiley and Sons, Inc., Wiley-Interscience Publication, 1973.
[27] E. Ivanova, K. Hadjiivanov, D. Klissurski, M. Bevilacqua, T. Armaroli, G. Busca, Microporous Mesoporous Mater. 46 (2001) 299.
[28] L.M. Cornaglia, J. Múnera, S. Irusta, E.A. Lombardo, Appl. Catal. A: Gen. 263 (2204) 91.
[29] T. Montanari, O. Marie, M. Daturi, G. Busca, Catal. Today 110 (2005) 339.
[30] E. Finocchio, et al. J. Mol. Catal. A: Chem. 535 (2003) 204–205.
[31] T. Montanari, O. Marie, M. Daturi, G. Busca, Appl. Catal. B: Environ. 71 (2007) 216.
[32] K. Hadjiivanov, G. Vayssilov, Adv. Catal. 47 (2002) 307.
[33] J.L. Macedo, S. Dias, J.A. Dias, Microporous Mesoporous Mater. 72 (2004) 119.
[34] M. Campa, I. Luisette, D. Pietrogiacomi, V. Indovina, Appl. Catal. B: Environ. 46 (2003) 511.
[35] E.L. Rodriguez, J.M.C. Bueno, Appl. Catal. A: Gen. 232 (2002) 147.
[36] J. Stencel, V. Rao, J. Diehl, K. Rhee, A. Dhere, R. DeAngelis, J. Catal. 84 (1983) 109.
[37] Barbara Ernst, Suzanne Libs, Patrick Chaumette, Alain Kiennemann, Appl. Catal. A: Gen. 186 (1999) 145–168.
[38] T.H. Fleish, R.F. Hicks, A. Bell, J. Catal. 87 (1984) 398.
[39] G. Gallaher, J.G. Goodwin, C. Huang, M. Houalla, J. Catal. 140 (1993) 453.
[40] W. Grünert, U. Sauerlandt, R. Schlögl, H.G. Karge, J. Phys. Chem. 97 (1993) 1413.
[41] A. Martínez-Hernández, G.A. Fuentes, Appl. Catal. B: Environ. 57 (2004) 167.
[42] J. Dědeček, B. Wichterlová, J. Phys. Chem. B 103 (1999) 1462.
[43] D. Kaucký, J. Dědeček, B. Wichterlová, J. Catal. 194 (2000) 318.